International Journal of Mass Spectrometry 306 (2011) 210–218

Contents lists available at ScienceDirect

International Journal of Mass Spectrometry

journal homepage: www.elsevier.com/locate/ijms

Thermal decomposition of *t*-amyl methyl ether (TAME) studied by flash pyrolysis/supersonic expansion/vacuum ultraviolet photoionization time-of-flight mass spectrometry

Thomas Hellman Morton*, Kevin H. Weber, Jingsong Zhang**

Department of Chemistry, University of California, Riverside, CA 92521-0403, United States

ARTICLE INFO

Article history:
Received 26 August 2010
Received in revised form 14 October 2010
Accepted 1 November 2010
Available online 9 November 2010

Dedicated to Tino Gäumann on the occasion of his 85th birthday.

Keywords:
Fuel oxygenate
Pyrolysis
Free radical
Bond homolysis
DFT
CCSD

ABSTRACT

Thermal decomposition of the oxygenated fuel component *tert*-amyl methyl ether (TAME) has been studied by flash pyrolysis up to 1250 K in a 20–100 μs time scale. Pyrolysis was followed by supersonic expansion to isolate intermediates and products, which are monitored by vacuum ultraviolet single-photon ionization time-of-flight mass spectrometry (VUV-SPI-TOFMS). The species detected, such as CH_3, C_2H_4, C_2H_5, C_4H_8, C_5H_{10}, C_3H_6O, and C_4H_8O, show competition between molecular elimination and bond fission pathways. The alkenes 2-methyl-1-butene (**1**) and 2-methyl-2-butene (**2**), the primary molecular elimination products of TAME, were separately pyrolyzed to evaluate the extent of secondary decompositions, as were the ketones (acetone and 2-butanone) produced by losses of two alkyl radicals. While vicinal elimination of methanol from TAME to form **1** and **2** in an approximate 3:1 ratio begins around 600 K and continues to dominate at higher temperatures, homolysis of TAME to form radicals onsets >825 K, yielding more acetone than 2-butanone. Contributions from secondary dissociations of the ketone and alkene products are evaluated.

1. Introduction

At the onset of World War I in the early 20th century it became critical to augment the power of spark-initiated internal combustion engines to make aviation possible. The fundamental limitation to increasing the compression ratio (and thus the power) for these engines was occurrence of "knock". Originally believed to occur during the compression stroke of the four-stroke engine, knocking or "pinging" was shown to result from pre-flame chain branching reactions during the power stroke [1]. When a fuel mixture decomposes in an uncontrolled manner ahead of the desired flame front, a sharp spike in pressure results, offset from the power stroke, which rapidly destroys the engine cylinder head and piston. Many molecules were found to prevent knocking (*e.g.*, iodine). Although aniline was found to have superior anti-knock properties, the organometallic compound tetraethyllead (TEL) proved to be most practical [2] and was rapidly incorporated as an anti-knock additive to gasolines. The widely used octane number indicates the extent of anti-knock properties of a fuel for spark-ignition motors. By contrast, pro-knock additives confer an advantage for diesel engines.

Over the years, concerns about automobile emissions have increased. As catalytic converters were introduced in the 1970s, methyl *tert*-butyl ether (2-methoxy-2-methylpropane, MTBE) became employed as an anti-knock additive, being an affordable and cleaner burning replacement for TEL, which was not compatible with catalytic converters. MTBE, *tert*-amyl methyl ether (2-methoxy-2-methylbutane, TAME), and ethyl *tert*-butyl ether (2-ethoxy-2-methylpropane, ETBE) have since been used as components of more modern gasolines due to their anti-knock properties, reduced volatile organic compound emissions, lack of toxicity (relative to TEL), and cost-effectiveness.

Unfortunately, MTBE is somewhat soluble in water [3] and, because of its odor [4], can render ground water unpalatable at low concentrations. Incidents of leakage from underground storage tanks into water supplies have caused MTBE to be outlawed in many locales. As a result, higher homologues such as TAME (being approximately three times less water soluble than MTBE [5]) have been employed. Compounds that are even less soluble such as *tert*-octyl methyl ether (2-methoxy-2,4,4-trimethylpentane, TOME) [6,7], *tert*-hexyl methyl ether (2-methoxy-2,3-dimethylbutane,

* Corresponding author. Tel.: +1 951 827 4735; fax: +1 951 827 4713.
** Corresponding author at: Air Pollution Research Center, University of California, Riverside, CA 92521, United States. Fax: +1 951 827 4713.
E-mail addresses: morton@citrus.ucr.edu (T.H. Morton), jingsong.zhang@ucr.edu (J. Zhang).

1387-3806/$ – see front matter © 2010 Elsevier B.V. All rights reserved.
doi:10.1016/j.ijms.2010.11.003

MDMB) [8], and other homologues [9–14] have also been seriously considered as replacements for MTBE. Nevertheless, the smaller *tert*-butyl ethers TAME, ETBE, and MTBE continue to be used because of the facility of manufacture at the refinery and the ease of mixing with gasoline on site (although questions remain regarding their ecotoxicity [15]).

The anti-knock ability of *tert*-alkyl ethers has been ascribed to a propensity for thermal decomposition into alkene plus alcohol *via* concerted vicinal elimination. Both products themselves confer high octane. Eq. (1) depicts molecular elimination for the anti-knock compound TAME. The alkenes produced, **1** and **2**, can prevent knock by intercepting reactive radicals (particularly OH) in the cool-flame region, forming resonance-stabilized radicals, which are less reactive [16,17]. Conversely, this model implies that a fuel additive, which itself initiates free radical formation, will have a pro-knock effect. The present study continues this laboratory's explorations of temperature regimes where MTBE [18] and its higher homologues [19] undergo bond homolysis to generate methyl radicals.

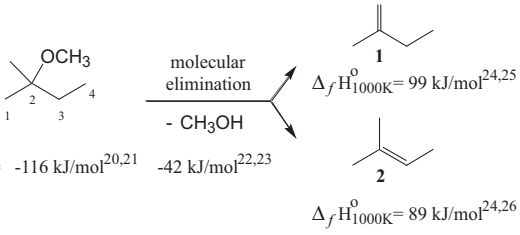

(1)

As Eq. (1) summarizes, molecular elimination from TAME is endothermic by $\Delta H = 60–70\ \mathrm{kJ\,mol^{-1}}$ at 1000 K, depending on the hydrocarbon product [20–27]. The entropy change for splitting one molecule into two has a positive value, giving a value on the order of $T\Delta S_{1000} = -105\ \mathrm{kJ\,mol^{-1}}$ for Eq. (1). In other words, molecular elimination at 1000 K has a negative ΔG.

2. Background

Thermal decomposition of a variety of alkyl ethers has been studied using static and flow reactors, as well as shock tubes. Among primary alkyl ethers, dimethyl ether decomposes via bond homolysis to give free-radicals [28–31], while methoxyethane [32] and diethyl ether exhibit both homolysis and molecular elimination [33–37]. Shock tube studies monitor bond homolysis in the presence of oxygen at high temperatures by looking at hydroxyl radicals produced via the sequence shown in Eq. (2).

$$CH_3OR \xrightarrow{-R^\bullet} CH_3O^\bullet \xrightarrow{-CH_2=O} H^\bullet \xrightarrow{\text{added } O_2} HO^\bullet \qquad (2)$$

Eq. (2) depicts a strategy for indirectly measuring the production of methoxy radicals and other intermediates that lose a hydrogen atom, but it does not detect methyl radicals. Methoxy radicals dissociate to formaldehyde plus hydrogen atoms, and these atoms react with added oxygen to produce hydroxyl radicals, which are monitored by laser-induced fluorescence. In the present work, 118.2 nm photoionization of the pyrolysis products provides direct observation of methyl radicals, although this technique cannot detect hydrogen atoms, formaldehyde, carbon monoxide, or other species with ionization energies above 10.5 eV. At temperatures ≥1000 K, the pyrolysis/supersonic jet/photoionization method used here provides an approach complementary to shock tube studies.

Competition between molecular elimination and bond homolysis depends on temperature. Molecular eliminations dominate thermal decomposition pathways at moderately elevated temperatures, because they have lower activation energies, but at higher temperatures the more favorable activation entropy of a simple bond homolysis compensates for the higher activation energy. Eq. (3) illustrates the molecular elimination in competition with bond cleavages that generate methyl radicals. The uppermost pathway represents elimination via a 4-center cyclic transition state, while the lower two depict typical homolyses.

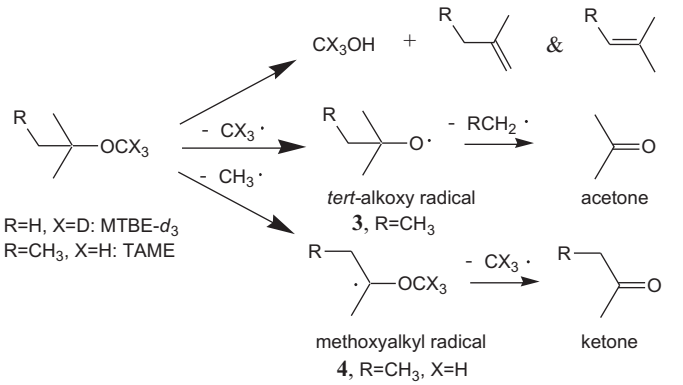

(3)

Below 950 K, diisopropyl ether (a secondary alkyl ether) decomposes mainly by molecular elimination [38], while the tertiary alkyl ethers MTBE [39–48], TAME [44–46,48], and ETBE [43–46] have been reported to react nearly exclusively *via* molecular elimination. Measurable levels of bond homolysis in methyl *tert*-alkyl ethers begin to emerge at around 950 K, becoming visible by the detection of methyl radicals among the pyrolysis products, as observed by photoionization mass spectrometry [18,19,47]. A peculiarity of this pathway is the difficulty in seeing the concomitant radical species, *tert*-alkoxy or methoxyalkyl radicals, illustrated in Eq. (3). In the case of MTBE, the methoxymethyl cation contributes the base peak in the mass spectrum of the parent neutral, so it becomes virtually impossible to ascertain whether this ion arises from photoionization of neutral MTBE or of radical intermediates.

As the uppermost pathway in Eq. (3) depicts, the hydrocarbon from molecular elimination product of MTBE, isobutene, appears first and persists in competition with bond homolysis up to temperatures at which it, too, undergoes thermal decomposition. Eq. (1) illustrates the corresponding products from TAME. On the one hand, isomers **1** and **2** should form in a 3:1 ratio based on purely statistical considerations of the number of vicinal hydrogen atoms. On the other hand, thermochemistry favors **2**: the **1** ⇋ **2** equilibrium proportions in the gas phase have been measured to as 7.5:92.5 at room temperature [20] and should have a value on the order of 35:65 at 1000 K [24–26].

As the lower pair of pathways in Eq. (3) depict, *tert*-alkoxy or methoxyalkyl radicals such as $RCH_2CMe_2O^\bullet$ or $CD_3OCMeCH_2R^\bullet$ ought readily to expel a molecule of ketone to yield a methyl radical ($CH_3^\bullet$ or $CD_3^\bullet$, respectively). The observation of both *m/z* 15 and *m/z* 18 from photoionization of pyrolysis products of MTBE-d_3 corroborates that expectation [18,19]. Although acetone is reported in the shock tube study of MTBE, this product is seen under flash pyrolysis conditions to a lesser extent than might have been anticipated on the basis of the stoichiometry $Me_3COMe \rightarrow Me_2C{=}O + 2CH_3^\bullet$ [18,19,48]. A 3:1 ratio of *m/z* 15 to *m/z* 18 from Me_3COCD_3 suggests that the acetone itself decomposes further to yield carbon monoxide and a net total of 4 methyl radicals.

The question arises as to why the ketone yield is low, even at the onset of bond homolysis. To that end, this study examines the pyrolysis of TAME, for which one of the molecular elimination products, 2-methyl-1-butene, **1**, ought to display less thermal stability than do acetone or 2-butanone, formed by two successive losses of free radicals. The 298 K C2–C3 bond dissociation energies of acetone and 2-butanone (based on the $\Delta_f H$ values for methyl radical [49],

ethyl radical [50] and acetyl radical [51]) are $\Delta H = 353$ kJ mol^{-1} and $\Delta H = 350$ kJ mol^{-1}, while the dissociation of **1** to give methallyl [52] plus methyl radicals has an endothermicity of $\Delta H = 308$ kJ mol^{-1}.

One therefore expects to see the ketone products and C_5H_{10} concurrently from pyrolysis of TAME at the onset of bond homolysis. As will be described below, experimental evidence indicates that **1** constitutes the major isomer from molecular elimination. Yet TAME does not yield ketones to the extent expected on the basis of stoichiometry under conditions where pyrolysis produces radicals.

This leads to a variety of plausible suppositions. Surface catalysis represents one possibility, a consideration that applies to all gas phase pyrolyses (with the exception of shock tube studies). Perhaps the hot surface catalyzes bond homolysis, so that radical products stick to it, and additional surface catalysis degrades the ketones further, as Eq. (4) depicts. Even if ketone decomposition does not undergo surface catalysis, adhesion of the precursor radicals would increase contact time, giving those products a longer period in which to dissociate. Further consideration of the role of surface chemistry lies outside the scope of the present study (except to note that the consequences of radical formation in an automobile cylinder do not depend on the homogeneity of the reaction).

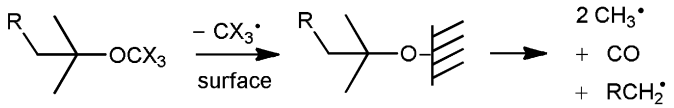

R=H, X=D: MTBE-d_3
R=CH_3, X=H: TAME

surface-bound alkoxy group

(4)

Alternatively, if bond homolysis does occur homogeneously in the gas phase, ketones from the second steps of Eq. (3) might be formed with internal vibrational excitation. Because (as mentioned below in Section 5) shock tube studies confirm the formation of methyl radicals via a homogeneous gas phase reaction, this interpretation appears as the most reasonable explanation at the present moment.

The objectives here include an experimental estimate of the yield of neutral radicals and of ketones from pyrolysis of TAME, as well as a theoretical evaluation of the vibrational excitation that might accompany further radical loss from an intermediate radical (the second step of the lower pair of pathways in Eq. (3)). While the results in hand do not rule out any of the aforementioned options, they do place constraints on the homogeneous gas phase pathway.

A relatively limited amount of published experimental data document the pyrolysis of TAME. Oxidation of TAME has previously been observed by static reactor [43,44], high pressure jet-stirred reactor [45], and in non-premixed flame [46]. The dominant decomposition reaction over intermediate temperatures (700–1000 K) produces 2-methyl-1-butene (**1**) and 2-methyl-2-butene (**2**) with concomitant formation of methanol *via* the molecular elimination. Homolytic bond scissions become competitive at higher temperatures. The molecular elimination product branching distribution, treated thus far as completely statistical, is further investigated here.

The experimental approach – flash pyrolysis coupled to supersonic expansion and vacuum ultraviolet (VUV) photoionization mass spectrometry – offers short reaction times to examine the initial steps of the thermal decomposition, supersonic cooling to quench the subsequent reaction and to minimize recombination of the initial products and intermediates, and "soft" VUV photoionization to minimize ion fragmentation allowing for direct detection of transient intermediates. Quantum chemical calculations of bond homolyses assist in elucidating the most likely reaction pathways and provide a prelude to the experimental results.

3. Experimental

The thermal decomposition experiments were performed with an apparatus that has been previously described [18]. Briefly, it makes use of a Wiley–MacLaren type linear time-of-flight mass spectrometer to observe pyrolysis products by means of 118.2 nm photoionization. TAME (99+%) and 2-methyl-2-butene (99+%) were obtained from Sigma–Aldrich. 2-Methyl-1-butene (99+%) was obtained from Columbia Organic Chemicals. Samples were used without further purification and introduced to the pyrolytic apparatus diluted in helium, argon, carbon tetrafluoride, or sulfur hexafluoride by bubbling the carrier gas through the liquid. The backing pressure of the gas mixture was maintained at approximately 1.5 atm for all experiments.

The pyrolysis micro-reactor is based on the design described by Chen and co-workers [53]. Thermal decompositions are carried out by expanding the gas mixture through a heated SiC nozzle (Carborundum, heated length 10 mm, 2 mm o.d., 1 mm i.d.) attached to a machinable alumina piece that isolates the nozzle thermally and electrically from the pulsed valve. The nozzle is heated resistively by means of two press-fitted graphite electrodes with the current controlled by a Variac transformer. The temperature of the nozzle was measured with a type C (Omega) thermocouple attached to the exterior of the reaction zone, which had previously been calibrated to the internal temperature. The reliability of the temperature measurement for the nozzle has been investigated previously [19] and was determined to be accurate to ±50 K. The speed of the sample flow was shown to be approximately sonic with a residence time of around 20–100 μs depending on the carrier gas utilized [53,54]. Upon exit from the heated reaction zone the nascent products, intermediates, and any remaining reactants undergo supersonic expansion, which significantly reduces their internal energy content [55]. A molecular beam extracted from this expansion is then intercepted by 118.2 nm photons (10.49 eV) produced by frequency tripling of the 355 nm third harmonic of a Nd:YAG laser in a Xe cell (approximately 20 Torr). The 118.2 nm light is focused by a MgF_2 lens through a small aperture into the photoionization region with concomitant divergence of the fundamental 355 nm source to minimize multiphoton ionization. TOF spectra are collected using a multichannel plate detector and a digital oscilloscope with 512 laser shots averaged and then converted to mass spectra.

Energetics of selected species involved in the decomposition of TAME were calculated using the Gaussian03 program suite [56]. Geometries were optimized using the cc-pVTZ basis set by means of the B3LYP hybrid density functional theory method [57], with harmonic normal modes calculated at the same level of theory. Single-point calculations of electronic energies using CCSD/cc-pVTZ were carried out on the B3LYP/cc-pVTZ optimized structures.

4. Results

Setting aside its CHs, TAME possesses five nonequivalent single bonds, of which four are calculated to have comparable bond dissociation energies (the fifth, the C3–C4 bond, is much stronger, and its cleavage will not be further discussed). Table 1 summarizes computations at two levels, including CCSD single point calculations using the B3LYP/cc-pVTZ geometries. The calculations here focus on the relative energies of the four competing homolytic pathways and the barriers for loss of methyl radicals from intermediates **3** and **4** to yield 2-butanone. As can be seen, the ordering of homolytic thermochemistries differs substantially between the B3LYP and CCSD levels. The CCSD calculations predict the *O*-methyl bond to have the lowest dissociation energy, consistent with previously published calculations on MTBE [58]. In other words, CCSD predicts

Table 1
Electronic energies (in a.u.) of radicals from competing bond homolyses of TAME and of transition states for radical expulsions from **3** and **4**, along with zero point energies and relative 1000 K bond dissociation energies (in kJ mol^{-1}), as well as 0 K activation barriers for the radical expulsions.

Process	B3LYP	ZPE	CCSD	E_{B3LYP}	E_{CCSD}	$E^{\ddagger}_{B3LYP}$	$E^{\ddagger}_{CCSD}$
Free Radicals							
$C_2H_5C(CH_3)_2O$ (**3**)	-272.422446	393.81	-271.803287	0	0		
CH_3	-39.858672	77.88	-39.756259				
$C_2H_5C(CH_3)OCH_3$ (**4**)	-272.423168	395.18	-271.798764	-1.5	12.3		
C_2H_5	-79.192230	154.99	-78.990426				
$CH_3OC(CH_3)_2$ (**6**)	-233.095907	320.03	-232.566785	-16.7	5.9		
OCH_3	-115.099376	94.76	-114.861986				
$C_2H_5C(CH_3)_2$ (**5**)	-197.185711	379.74	-96.693841	-13.4	6.1		
Transition States							
3 → $[C_2H_5C(CH_3)_2O]^{\ddagger}$ → 2-butanone + CH_3	-272.401212	383.92	-271.774728			46.8	48.2
4 → $[C_2H_5C(CH_3)OCH_3]^{\ddagger}$ → 2-butanone + CH_3	-272.392154	381.46	-271.757650			68.7	94.2
3 → $[C_2H_5C(CH_3)_2O]^{\ddagger}$ → acetone + CH_2CH_3	-272.407300	385.55	-271.778917			32.5	38.9

that formation of *t*-amyloxy radical, **3**, represents the lowest energy homolytic cleavage of TAME.

The transition state calculations show barriers for subsequent radical loss. The bottom pathway in Eq. (4) (loss of methyl from **4**) has a much higher activation energy than do the dissociations of **3**. Thermodynamically, expulsion of ethyl radical from **3** to give acetone has a ΔH°_{298} of 5 kJ mol^{-1} less endothermic than does expulsion of methyl radical to give 2-butanone, but the barrier heights differ by 9–14 kJ mol^{-1} (depending on the level of computation). In the transition state calculated for methyl loss from **3**, the radical carbon lies 2.106 Å away from C2, while the transition state for ethyl loss has a shorter distance, 2.074 Å. With regard to energetics, the difference between those two transition states implies a greater yield of acetone than of 2-butanone from dissociation of intermediate **3**. The computational results parallel the data seen experimentally for the TAME molecular ion, which exhibits a reverse activation barrier for methyl loss greater than for ethyl loss, such that the latter fragmentation has a lower appearance energy (even though it is more endothermic) and a greater abundance at ionizing energies above threshold [59].

4.1. Pyrolysis of tert-amyl methyl ether (TAME)

Fig. 1A and B presents stack plots of mass spectra for the low temperature pyrolysis, up to 1000 K of TAME seeded in argon and sulfur hexafluoride, respectively. In Fig. 1A, with the nozzle at room temperature, a molecular ion is barely detectable ($M^{+\bullet}$ = *m*/*z* 102 for TAME), which has not previously been observed by mass spectrometry. A large $M-CH_2CH_3^+$ ion base peak at *m*/*z* 73 is observed accompanied by a $M-CH_3^+$ peak at *m*/*z* 87 having 8% of the base peak intensity. As mentioned above, photoionization of TAME shows that the thermodynamically more favorable dissociation to *m*/*z* 87 has a higher appearance energy (AE) than for *m*/*z* 73: AE (*m*/*z* 73) = 9.25 eV and AE (*m*/*z* 87) = 9.36 eV [59]. Even at photon energies well above threshold, ionized TAME fragments with preference for expulsion of the larger alkyl group, as also observed experimentally with other tertiary alkyl methyl ethers [18,19].

In Fig. 1A, a trace amount of 2,3,3-trimethyl-1-butene used to facilitate mass calibration is observed as a small $M^{+\bullet}$ peak at *m*/*z* 98 and, as the nozzle temperature is increased, its $M-CH_3^+$ peak at *m*/*z* 83 is also discernible. A small peak at *m*/*z* 78 is also noted, residual C_6H_6 produced from these pyrolysis experiments at higher temperatures. With a nozzle temperature of 575 K, the intensity of the *m*/*z* 73 peak from photoionization of the parent TAME decreases, while the intensity at *m*/*z* 87 (also from TAME) remains approximately the same. A new peak at *m*/*z* 70 with approximately 20% the intensity of the *m*/*z* 73 peak is now detected, corresponding to hydrocarbons **1** and **2**. These are the molecular elimination products of TAME (see Eq. (1)). Methanol produced concomitantly by same process has an IE (10.85 eV) [60] that exceeds the photoionization energy employed and hence cannot be seen. The peaks associated with the trace impurities diminish in intensity except for the *m*/*z* 83 fragment from 2,3,3-trimethyl-1-butene, which now becomes visible. When the nozzle is further heated to temperatures of 875 and 950 K the intensities of *m*/*z* 73 and *m*/*z* 87 steadily decrease as the parent compound is consumed. The product peak at *m*/*z* 70 grows to roughly one half, then nearly equal intensities with respect to TAME's base peak at *m*/*z* 73. Small peaks at *m*/*z* 55 and 56 become discernible, as well as small peaks at *m*/*z* 15, corresponding to CH_3 radical, and product acetone at *m*/*z* 58. At 1000 K, the $M-CH_3^+$ ion peak of TAME at *m*/*z* 87 is barely detectable and *m*/*z* 70 has increased to nearly double the intensity of $M-CH_2CH_3^+$ ion peak at *m*/*z* 73. The *m*/*z* 56 peak has grown in relative intensity to *m*/*z* 55. Small peaks at *m*/*z* 58 and *m*/*z* 72 are detectable, corresponding to the oxygenated products acetone (C_3H_6O) and 2-butanone (C_4H_8O), as well as at *m*/*z* 68 corresponding to isoprene, C_5H_8. A series of small peaks over *m*/*z* 40–43 are observed and the *m*/*z* 15 CH_3 peak intensity increases.

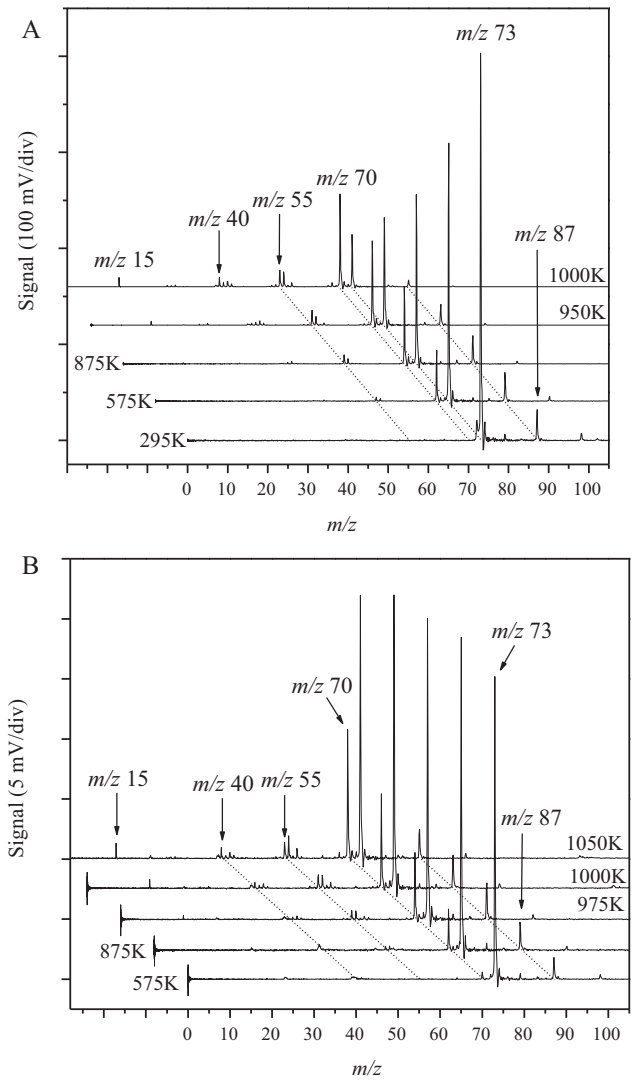

Fig. 1. (A) Stack plot of mass spectra for pyrolysis of TAME in argon with internal nozzle temperatures from near room temperature (295 K) to 1000 K. (B) Stack plot of mass spectra for pyrolysis of TAME in sulfur hexafluoride with internal nozzle temperatures from 575 K to 1050 K. The mass spectra are shifted for clarity.

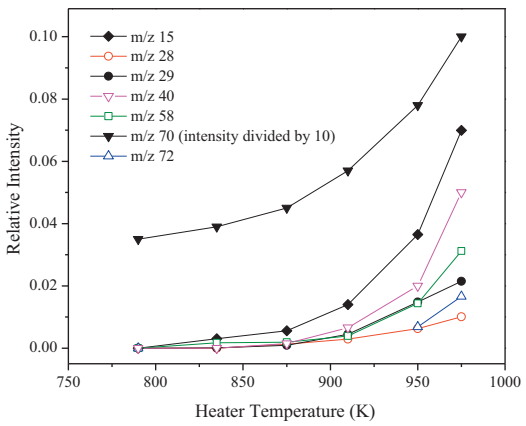

Fig. 2. Intensities of selected fragment ions (relative to *m*/*z* 73) from pyrolysis of TAME in argon below 1000 K.

Fig. 1B presents a stack plot of mass spectra for the pyrolysis of TAME with sulfur hexafluoride as the carrier gas. Although not pictured here, the room temperature spectrum produces a $M-CH_3^+$ peak with 8% of the intensity of the $M-CH_2CH_3^+$, the same relative intensity observed in the argon entrained sample. At a nozzle temperature of 595 K the product peak at *m*/*z* 70 is barely discernible, while at this nozzle temperature in argon, the *m*/*z* 70 peak has already reached about 20% of the *m*/*z* 73 base peak. The $M-CH_3^+$ ion peak at *m*/*z* 87 is found to have approximately 10% of the intensity of the *m*/*z* 73 $M-CH_2CH_3^+$ ion peak, similar to the argon data in Fig. 1A. With the higher nozzle temperature of 875 K, the *m*/*z* 70 product peak grows to roughly 10% of the *m*/*z* 73 intensity while *m*/*z* 87 and *m*/*z* 73 peaks remain essentially unchanged. Nozzle temperatures of 975, 1000, and 1050 K do not significantly change the intensities of *m*/*z* 73 and *m*/*z* 87 while the peaks from **1** and **2** at *m*/*z* 70 increases to greater than half of the *m*/*z* 73 peak intensity. New peaks at *m*/*z* 15, 40–43, 55, 56, and 58 are now clearly detected and, at 1050 K, a small peak at *m*/*z* 68 is observed.

The carrier gas was changed to examine the effect on the pyrolysis due to (1) different residence times in the microreactor, (2) heat capacities of carrier gas, and (3) cooling efficiency of the gas. The velocity at the throat of the expansion is approximately sonic, having an estimated residence time of 20 μs with helium as a carrier gas [53]. Since the speed should track inversely with square root of mass, the residence times of argon, carbon tetrafluoride and sulfur hexafluoride ought to be approximately three, five, and six times longer, respectively. With helium as a carrier gas the pyrolysis of TAME onsets at temperatures >600 K (data not shown here); however, with argon carrier gas pyrolysis onsets below 600 K (Fig. 1A). At a nozzle temperature of 875 K the intensity of *m*/*z* 70 relative to *m*/*z* 73 is approximately 25% in helium and 50% in argon. The cooling efficiency for these gases are similar and, as their heat capacities are virtually the same, the difference in the onset and extent of pyrolysis must be due to the different residence times. At temperatures >950 K the spectra using helium or argon are indistinguishable. For the polyatomic halogenated gases the presence of internal degrees of freedom increases heat capacities relative to the monoatomic gases. Residence times are longer, and the onset and extent of pyrolysis are significantly delayed compared to inert gas carriers. With sulfur hexafluoride as a carrier gas the onset of pyrolysis does not start until temperatures >600 K (Fig. 1B), and, at a nozzle temperature of 1050 K, the *m*/*z* 70 product peak is only roughly one half the *m*/*z* 73 parent ion intensity, while in helium and argon *m*/*z* 73 peak is greatly reduced. The $[M-CH_3]^+$:$[M-CH_2CH_3]^+$ ion ratio (*m*/*z* 87:*m*/*z* 73) for pyrolyses in helium, argon, carbon tetrafluoride, and sulfur hexafluoride carrier gases were determined. Within experimental error all carrier gases give the same ratio of photoionization fragmentation, with the $[M-CH_3]^+$ ion having 13 ± 4% the intensity of the $[M-CH_2CH_3]^+$ ion, consistent with previous mass spectrometric studies [59]. While the onset temperature for pyrolysis and the extent of reaction do differ (as indicated by comparing Fig. 1A and B), argon was chosen as the carrier gas for subsequent experiments to produce best quality spectra.

Fig. 2 summarizes the relative abundances of significant pyrolysis products formed in argon at temperatures <1000 K relative to the *m*/*z* 73 base peak from ionization of TAME. While molecular elimination of methanol (giving *m*/*z* 70) clearly dominates, radicals from homolysis (*m*/*z* 15 and *m*/*z* 29) start to be observed at 835 K, as does acetone (*m*/*z* 58), which results from the successive loss of methyl and ethyl groups from TAME (the middle pathway in Eq. (3)). Because it lies between *m*/*z* 70 and *m*/*z* 73, the mass spectrometric peak corresponding to 2-butanone (*m*/*z* 72, corresponding to loss of two methyls from TAME) emerges from background at higher temperatures, but it has an intensity approximately half that of acetone. As Section 5 will note, these ketones exhibit an abundance less than one would expect based on the observed intensities of methyl and ethyl radicals.

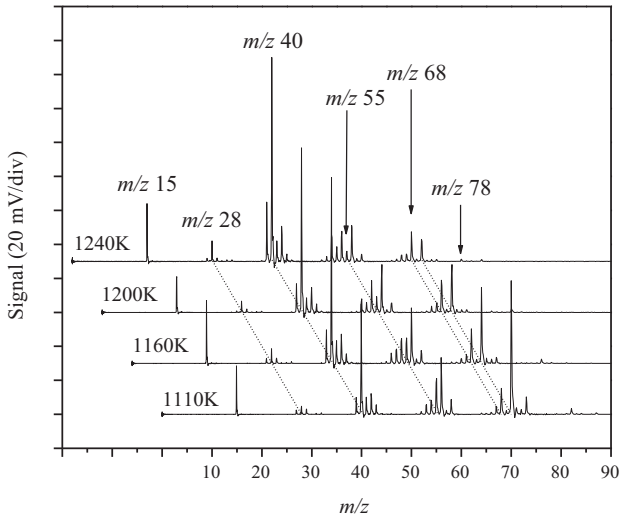

Fig. 3. Stack plot of mass spectra for pyrolysis of TAME in argon with internal nozzle temperatures from 1100 K to 1240 K.

Overlap with other symbols in Fig. 2 obscures the fact that methyl and ethyl radicals onset at the same temperature. At a slightly higher temperature (875 K) a m/z 28 appears, which corresponds to loss of a hydrogen atom from the ethyl radical. Above 900 K the m/z 28 peak displays an intensity roughly half that of m/z 29. Because ethylene has an IE (10.514 eV) very close to the energy of the 118.2 nm photons used in these experiments, it seems probable that ethylene has an abundance substantially greater than indicated by the intensity of its peak in the photoionization mass spectrum.

Fig. 3 presents a stack plot for the high temperature pyrolysis (1110–1250 K) of TAME seeded in argon. Above 1000 K, the m/z 28 peak starts to increase relative to m/z 29 peak, and above 1100 K the m/z 28 intensity exceeds that of m/z 29. At 1100 K little m/z 73 is detected, being approximately 10% of the m/z 70 product (C_5H_{10}) peak. The intensity of the peak at m/z 40, C_3H_4, increases drastically to nearly the same intensity as m/z 70, while the signals at m/z 15 (methyl radical), m/z 54 (C_4H_6), m/z 56 (C_4H_8), and m/z 68 (C_5H_8), have all increased in intensity. The production of C_4H_8 and a portion of the CH_3 signal is due to pyrolysis of TAME, while the other signals are known products from the pyrolysis of the C_5H_{10} hydrocarbons (*vide infra*) [46]. As the heater is raised to the higher temperatures of 1160, 1200, and 1240 K the m/z 70 peak steadily decreases in intensity, and in the highest temperature trace, 1240 K, m/z 78 is detected, corresponding to C_6H_6 (plausibly from the self combination of m/z 39 C_3H_3 radicals). The peaks at m/z 15, 28, and 40 continue to become more intense. The isobutylene peak at m/z 56 begins to slightly decrease in intensity, while new peaks over the m/z range of 52–54 are observed. At these higher temperatures the m/z 68 peak remains relatively constant and the m/z 73 peak from TAME is hardly detectable. Arrhenius behavior would predict the half life for TAME [44,45] at a temperature of 1200 K to be on the order of 70–150 μs with respect to molecular elimination, which is comparable to the estimated residence time of 60 μs for argon. Experimentally, TAME is found here to decompose completely at this temperature: the M−CH_3 ion at m/z 87 and M−CH_2CH_3 ion at m/z 73 corresponding to the photoionization fragments of TAME are not observed >1200 K.

4.2. Pyrolyses of 2-methyl-1-butene (**1**) and 2-methyl-2-butene (**2**)

In order to evaluate the contribution of product fragmentation and investigate relative product yields, pyrolyses of hydrocarbons

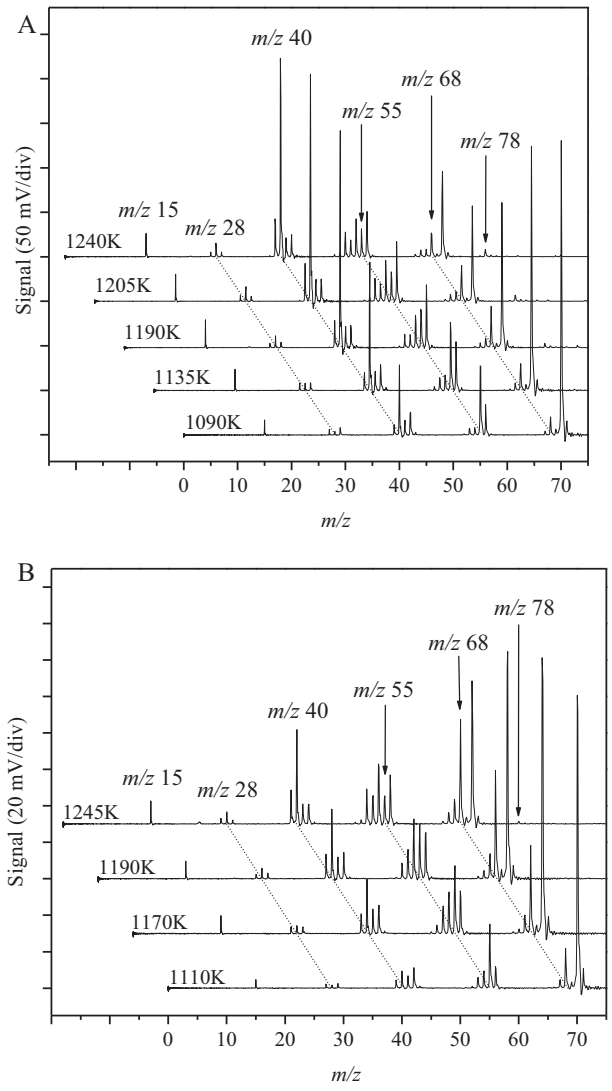

Fig. 4. (A) Stack plot of mass spectra for pyrolysis of 2-methyl-1-butene (**1**) in argon with internal nozzle temperatures from 1090 K to 1240 K. (B) Stack plot of mass spectra for pyrolysis of 2-methyl-2-butene (**2**) in argon with internal nozzle temperatures from 1110 K to 1245 K.

1 and **2** in argon carrier gas were conducted. Fig. 4A and B presents stack plots of mass spectra for temperatures from 1100 to 1250 K. When comparing the two isomers in Fig. 4 the mass spectrometric patterns of **1** and **2** undergoing pyrolysis shows significant differences. Relative to the molecular ion signal at m/z 70, a large amount of m/z 68 is produced in the pyrolysis of **2** compared to **1**. This is explained by the propensity of **2** to undergo molecular decomposition to evolve hydrogen gas via 1,4-elimination and produce 2-methyl-1,3-butadiene (isoprene) in preference to radical decomposition. The pyrolysis of **1**, on the other hand, produces a greater amount of signal at m/z 40, C_3H_4, via loss of the elements of ethane. Cleavage of a methyl radical to form methallyl radical followed by subsequent loss of a second methyl radical provides a reasonable explanation for m/z 40, predicting that the isomer thus produced has the structure of allene.

Although the two alkenes have distinguishably different pyrolysis spectra, a pair of obstacles limits an accurate determination of the ratio of the product C_5H_{10} isomers in the pyrolysis of TAME: (1) differences in residence time for products compared to authentic samples and (2) interference from competing pyrolytic processes. In an attempt to determine the product isomer branching ratio from

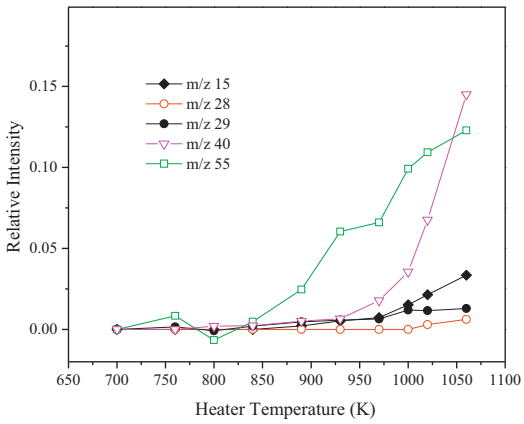

Fig. 5. Intensities of selected fragment ions relative to the molecular ion at *m*/*z* 70 (minus peak intensities at temperatures below 700 K) from pyrolysis of 2-methyl-1-butene (**1**) in argon.

the TAME pyrolysis, the relative amounts of *m*/*z* 40 and *m*/*z* 68 in sample mixtures composed of 0%, 25%, 50%, and 100% **1** in **2** were pyrolyzed and compared with the spectra TAME at higher temperature (Fig. 3). It was apparent that the majority of molecular elimination product is **1**, consistent with the previous study [44]. This comparison suggested a branching ratio value of 75 ± 20% **1** from TAME. Another noticeable differentiation between the **1** and **2** is the amount of *m*/*z* 78 observed. In Fig. 4A, pyrolysis of **1**, a signal at *m*/*z* 78 is detected at temperatures ≥1190 K. In the pyrolysis of **2** presented in Fig. 4B, a signal at *m*/*z* 78 is only barely detected in the hottest temperature trace at 1245 K, because **2** undergoes molecular elimination of H_2 in preference to C_3H_4 (*m*/*z* 40) production. Conversely, **1** prefers to decompose to C_3H_4 and can then lose a H atom to form propargyl radicals, which then combine to form C_6H_6 [61].

Comparing Fig. 4A and B to Fig. 3 it is apparent that the high-temperature pyrolysis of TAME produces mass spectra similar to those produced by pyrolysis of **1** and **2**. The most noticeable differences distinguishing the TAME data from the C_5H_{10} pyrolysis experiments, however, are greater abundances of *m*/*z* 15, 28, and 56 from TAME. Fig. 5 summarizes the behavior of 2-methyl-1-butene (**1**) at the lower temperatures at which it begins to decompose.

Fission of the sp^3–sp^3 carbon–carbon bond of **1** to form methallyl radical represents the least endothermic homolysis pathway, but the *m*/*z* 55 ion also corresponds to the base peak in the photoionization mass spectra of **1** and **2**. The emergence of this ion between 835 and 890 K above that substantial background in Fig. 5 (which corrects for the presence of that peak in the mass spectrum of **1**) is taken to signal the onset of dissociation of neutral **1**. The formation of methyl radicals (*m*/*z* 15, which contributes a negligible peak to the photoionization mass spectrum) ought to accompany homolysis of **1** but does not become visible above noise level until 930 K and, as Fig. 4A shows, exhibits an intensity equal to that of *m*/*z* 55 only above 1200 K. This discrepancy could be attributed to the difference in 118.2 nm photoionization cross sections of the two radicals.

Loss of the elements of ethane to yield C_3H_4 (*m*/*z* 40, which also corresponds to a negligible peak in the mass spectra of **1** and **2**) provides another gauge of thermal decomposition of neutral **1**. This dissociation, which can be attributed to further loss of methyl radical from the methallyl radical, also emerges between 835 and 890 K, the same onset temperature (within experimental uncertainty) as in the pyrolysis of TAME (as Fig. 2 summarizes). In the case of TAME, however, molecular elimination has to occur prior to decomposition to C_3H_4, which implies that C_5H_{10} has a much shorter residence time under those conditions. This suggests that further dissociation of the alkenes produced by TAME is accelerated. The discussion below deals with conclusions based on this inference.

5. Discussion

The observation of *m*/*z* 15 and *m*/*z* 29 from the supersonic jet expansion/photoionization of TAME pyrolysis products testifies as to the formation of radicals from bond homolysis. A recent shock tube study [47], which reports the formation of ethane from high temperature pyrolysis of MTBE, confirms the formation of methyl radicals from homogeneous gas phase decomposition of highly branched methoxyalkanes, as first described by this laboratory a decade ago [18]. Other products reported from gas chromatographic analysis of the shock tube products from MTBE also agree with those observed in the present study, especially allene and propyne (here observed as *m*/*z* 40 peaks). The peaks at *m*/*z* 40 also arise from pyrolysis of **1** and **2** via loss of the elements of ethane. This pathway is much more prominent for **1** than for **2**, consistent with the structural difference between those two isomeric alkenes.

Mass spectra of the pyrolysis products of TAME exhibit the same *m*/*z* 73: *m*/*z* 87 intensity ratio as seen from photoionization of TAME itself. In principle, three bond cleavages could generate free radicals having these masses: the loss of ethyl radical to yield $(CH_3)_2COCH_3$ (**6**, 73 amu) and the two pathways for methyl loss shown in Eq. (3) (to yield 87 amu radicals, **3** and **4**). Because it seems implausible that the proportions of bond cleavage of neutral TAME should so closely match the fragmentation pattern of ionized TAME, the aforementioned radicals are inferred to be largely absent.

As Table 1 summarizes, four bond homolyses can compete in the thermal dissociation of neutral TAME below 1000 K. DFT and CCSD calculations predict different orderings of the relative bond dissociation energies, but it appears that the pyrolyses to yield methyl radicals have thresholds comparable to the losses of methoxyl radical or ethyl radical. As Eq. (2) indicates, further dissociation renders methoxyl radical invisible under the experimental conditions used here. The concomitant *tert*-amyl radical, **5**, can dissociate via further loss of CH_3 to give isobutene (*m*/*z* 56), which (so far as can be ascertained from Fig. 1) exhibits an onset not far from the temperature at which *m*/*z* 15 and *m*/*z* 29 begin to emerge.

At elevated temperatures virtually all organic free radicals from bond homolyses (with the exception of methyl radical, C_nH_n, and other highly unsaturated analogues) dissociate via loss of a hydrogen atom or CH_3. This implies, in turn, that ketones – acetone and 2-butanone – ought to form. While ions at the appropriate masses (*m*/*z* 58 and *m*/*z* 72) do appear, they exhibit intensities lower than that of the concomitant methyl radicals at all temperatures. It is not easy to account for the discrepancy simply in terms of relative ionization cross sections.

According to the CCSD calculations in Table 1, the lowest energy pathway for TAME homolysis cleaves the C–O bond to produce **3**, which can then lose ethyl radical to give acetone (the middle pathway in Eq. (3)). Since *m*/*z* 15, *m*/*z* 29, and *m*/*z* 58 onset at the same temperature, the experimental results in Fig. 2 agree with this prediction, although the data do not permit an assessment of whether CH_3 or C_2H_5 comes off first. Shock tube studies of the thermal decomposition of acetone, if fit to the Arrhenius equation [62,63], predict that it should have a half-life for homogeneous dissociation at 1000 K on the order of 3–8 ms. While more recent studies [64] fit the data to non-Arrhenius behavior, acetone ought to remain stable much longer that the contact time in the present experiments. The following discussion interprets the comparatively low yields of acetone and of 2-butanone in terms of vibrational excitation remaining after expulsion of radicals in the second steps of Eq. (3).

To begin with, the evidence suggests that elimination of methanol from TAME produces vibrationally excited C_5H_{10}. As Fig. 2 indicates, the onset of *m*/*z* 40 from TAME at the same tem-

perature as in the pyrolysis of **1** summarized in Fig. 5, even though the C_5H_{10} residence time is substantially shorter in the former case. Loss of two successive methyl radicals from C_5H_{10} accounts for the formation of C_3H_4. In the TAME pyrolysis, as in the pyrolysis of **1** summarized in Fig. 5, m/z 40 appears at the same temperature as does m/z 55 (after subtracting the contribution to the intensity of latter from photoionization of C_5H_{10}). Close to onset the m/z 40:m/z 55 ratio has a value close to 0.15 in both cases. Because molecular elimination from TAME has an activation barrier $\geq$230 kJ mol^{-1} [44], much higher than the thermodynamic thresholds in Eq. (1), it comes as little surprise that the resulting alkenes can form with vibrational excitation that leads to decomposition rates faster than from thermal activation by itself. The question arises whether the same effect operates for the ketones formed from TAME.

Loss of alkyl radicals from intermediates **3** or **4** have calculated electronic energies close to zero, for which $\Delta\varepsilon_{vib}$ more than compensates at high temperatures (an effect attenuated somewhat by inclusion of $\Delta\varepsilon$ from molecular rotations): *e.g.*, at B3LYP/cc-pVTZ the exothermicity of methyl loss from **4** has a calculated value of $\Delta H^\circ = -37$ kJ mol^{-1} (taking into account the changes in ZPE and harmonic canonical energies). The computed activation energies summarized in the last three entries of Table 1 show surprisingly high barriers for further expulsion of radicals from radicals **3** and **4**. The excess internal energy from surmounting these barriers as well as the net exothermicities could enhance the rate of further dissociation of the resulting ketones.

The yield of m/z 15 near onset exceeds the combined yields of the C_2 fragments m/z 29 plus m/z 28. Although competing homolyses can also yield methyl radicals, the C_2 yield ought to equal that of acetone, but such is not the case <975 K. Since **3** and **4** have calculated activation barriers >30 kJ mol^{-1} for subsequent expulsion of alkyl radicals, their dissociation might partition a significant fraction of the excess energy into internal degrees of freedom of the ketones (as occurs for the molecular elimination leading to alkenes), giving rise to further decomposition and reducing ketone abundance below that expected on the basis of stoichiometry.

The transition state calculations in Table 1 predict that the *tert*-amyloxy radical ought to expel ethyl radical (to give acetone) more readily than methyl (to give 2-butanone). Expulsion of the *O*-methyl from 2-methoxy-2-butyl radical **4** (bottom path in Eq. (3)) offers yet another route to 2-butanone, but (as Fig. 2 summarizes) the yield of acetone from TAME pyrolysis is at least twice as great as that of 2-butanone. While this outcome is consistent with the computational prediction (and in agreement with the lower experimental appearance energy for formation of m/z 73 relative to m/z 87 from ionized TAME [59]), the facility with which the ketones might undergo subsequent decomposition under the experimental conditions stands in the way of a definitive confirmation.

In addition to the aforementioned rationalization of the low abundance the expected ketones, other products warrant further comment. TAME produces butenes, which might conceivably parallel the production of propene in the shock tube study of MTBE [47]. On the one hand, as noted above, loss of methoxyl from TAME to form $(CH_3)_2CCH_2CH_3$ radical **5** opens an avenue not available in the case of MTBE: simple loss of a methyl radical from **5** to produce $(CH_3)_2C{=}CH_2$. On the other hand, butenes also form in the pyrolysis of **1** and **2**, although to a lesser extent. Formation of C_4H_8 from C_5H_{10} could arise by methane loss via "roaming radicals", a possibility recently proposed for alkane pyrolyses [65]. Alternatively, the butenes from **1** and **2** may come from bimolecular reactions. One possibility supposes that addition of a hydrogen atom to **1** or **2** followed by loss of a methyl radical yields butenes (or that addition of a methyl radical to **2** followed by loss of an ethyl radical yields isobutene, with the ethyl radicals then losing a hydrogen atom quickly). These hypotheses remain to be tested.

6. Conclusion

Photoionization mass spectrometry of pyrolysis products reveals that thermal dissociation of neutral TAME in argon displays a threshold below 600 K, somewhat lower than the onset temperature for MTBE in argon (approximately 700 K) with the same experimental setup. Over the temperature range typically applicable to operation of an internal combustion engine (700–1000 K), molecular elimination of methanol to form 2-methyl-1-butene (**1**) and 2-methyl-2-butene (**2**) dominates, with a nearly a statistical distribution of products (3:1 ratio of 1–2). At temperatures >825 K the observation of methyl radicals indicates the onset of bond homolysis, as previously reported for MTBE. Ethyl radicals appear from TAME with the same threshold but tend to lose H$^\bullet$ to give ethylene at higher temperatures. Acetone, 2-butanone, and C_4H_8 also form via successive losses of two radicals, as does C_3H_4 from the C_5H_{10} products of molecular elimination. Acetone is more abundant than 2-butanone, implying that losses of ethyl and methyl from TAME occur with greater facility than loss of two methyls. That experimental result agrees with CCSD predictions of 39 and 48 kJ mol^{-1} activation barriers for expulsion of ethyl and methyl radicals, respectively, from the intermediate *tert*-amyloxy radical (**3**). Secondary decomposition of the ketones and of C_5H_{10}, which are not as robust as the isobutene formed from MTBE, takes place and appears to be accelerated as a consequence of the internal energy remaining after their formation.

Acknowledgments

This work was supported by the University of California Energy Institute and by NSF grants CHE-0848643 and CHE-0848517.

References

[1] T. Midgley Jr., Ind. Eng. Chem. 31 (1939) 504.
[2] T. Midgley Jr., T.A. Boyd, Ind. Eng. Chem. 14 (1922).
[3] A. Fischer, M. Muller, J. Klasmeier, Chemosphere 54 (2004) 689.
[4] X.L. Wang, M.A. Deshusses, Biodegradation 18 (2007) 37–50.
[5] R.M. Stephenson, J. Chem. Eng. Data 37 (1992) 80.
[6] M.J. Papachristos, J. Swithenbank, G.H. Priestman, S. Stournas, P. Polysis, E. Lois, J. Inst. Energy 64 (1991) 113.
[7] L.K. Rihko-Struckmann, R.S. Karinene, A.O.I. Krause, K. Jakobsson, J.R. Aittamaa, Chem. Eng. Process. 43 (2004) 57.
[8] J. Snelling, M.O. Barnett, D. Zha, J.S. Arey, Environ. Toxicol. Chem. 26 (2007) 2253.
[9] L.K. Rihko, A.O.I. Krause, Ind. Eng. Chem. 35 (1996) 2500.
[10] J. Liu, S. Wang, J.A. Guin, Fuel Process. Technol. 69 (2001) 205.
[11] D.E. Hendrickson, U.S. Patent Application W09516763.
[12] L.A. Smith, H.M. Putman, H.J. Semerak, C.S. Crossland, U.S. Patent 6,583,325.
[13] T. Evans, K.R. Edlund, U.S. Patent 2,010,356.
[14] J. Ignatius, H. Jaervelin, P. Lindqvist, Hydrocarbon Process. 74 (1995) 51.
[15] J. Bartling, M. Schloter, B.-M. Wilke, Biol. Fertil. Soils 46 (2010) 299.
[16] C.K. Westbrook, W.J. Pitz, Energy Technol. Rev. Feb/Mar (1991) 1.
[17] C.K. Westbrook, Chem. Ind. (UK) (1992) 562.
[18] S.D. Chambreau, J.S. Zhang, J.C. Traeger, T.H. Morton, Int. J. Mass Spectrom. 199 (2000) 17.
[19] K.H. Weber, J.S. Zhang, D. Borchardt, T.H. Morton, Int. J. Mass Spectrom. 249–250 (2006) 303.
[20] A. Heintz, S. Kapteina, S.P. Verevkin, J. Phys. Chem. B 111 (2007) 10975.
[21] A.M. Rozhnov, V.V. Safronov, S.P. Verevkin, K.G. Sharonov, V.I. Alenin, J. Chem. Thermodyn. 23 (1991) 629.
[22] J.H.S. Green, Chem. Ind. (UK) (1960) 1215–1216.
[23] S.S. Chen, R.C. Wilhoit, B.J. Zwolinski, J. Phys. Chem. Ref. Data 6 (1977) 105.
[24] K.B. Wiberg, S. Hao, J. Org. Chem. 56 (1991) 5108.
[25] J.R. Durig, G.A. Guirgis, D.A.C. Compton, J. Phys. Chem. 84 (1980) 3547.
[26] D.W. Scott, G. Waddington, J.C. Smith, H.M. Huffman, J. Am. Chem. Soc. 71 (1949) 2767.
[27] Heat capacity for TAME up to 1000 K estimated as described in S.W. Benson, Thermochemical Kinetics: Methods for the Estimation of Thermochemical Data and Rate Parameters, 2nd ed., Wiley-Interscience, 1976.
[28] K.H. Anderson, S.W. Benson, J. Chem. Phys. 36 (1962) 2320.
[29] D.J. McKenney, K.J. Laidler, Can. J. Chem. 41 (1963) (1984).
[30] Y. Hidaka, K. Sato, M. Yamane, Combust. Flame 123 (2000) 1.
[31] R.D. Cook, D.F. Davidson, R.K. Hanson, J. Phys. Chem. A 113 (2009) 9974.

[32] K. Yasunaga, T. Koike, H. Hoshikawa, Y. Hidaka, Proc. Combust. Inst. 31 (2007) 313.
[33] G.R. Freeman, C.J. Danby, C.N. Hinshelwood, Proc. R. Soc. A245 (1958) 28.
[34] C.J. Danby, G.R. Freeman, Proc. R. Soc. A245 (1958) 41.
[35] G.R. Freeman, Proc. R. Soc. A245 (1958) 75.
[36] K.J. Laidler, D.J. McKenney, Proc. R. Soc. A278 (1964) 505.
[37] A.T. Blades, G.W. Murphy, J. Am. Chem. Soc. 78 (1952) 1039.
[38] N.J. Daly, V.R. Stimson, Aust. J. Chem. 19 (1966) 239.
[39] N.J. Daly, C. Wentrup, Aust. J. Chem. 21 (1968) 1535.
[40] N.J. Daly, C. Wentrup, Aust. J. Chem. 21 (1968) 2711.
[41] K.Y. Choo, D.M. Golden, S.W. Benson, Int. J. Chem. Kinet. 6 (1974) 631.
[42] J.C. Brocard, F. Baronnet, Oxid. Commun. 1 (1980) 321.
[43] B. El Kadi, F. Baronnet, J. Chim. Phys. 92 (1995) 706.
[44] H. Bohm, F. Baronnet, B. El, Kadi, Phys. Chem. Chem. Phys. 2 (2000) (1929).
[45] A. Goldaniga, T. Faravelli, E. Ranzi, P. Dagaut, M. Cathonnet, Twenty-seventh Symposium (International) on Combustion/The Combustion Institute, 1998, pp. 353–360.
[46] C.S. McEnally, L.D. Pfefferle, Int. J. Chem. Kinet. 36 (2004) 345.
[47] K. Yasunaga, Y. Hidaka, A. Akitomo, T. Koike, 26th International Symposium on Shock Waves, vol. 1, 2009, p. 177.
[48] T.C. Zhang, J. Wang, T. Yuan, X. Hong, L.D. Zhang, F. Qi, J. Phys. Chem. A 112 (2008) 10487.
[49] D.J. Grant, D.A. Dixon, J. Phys. Chem. A 113 (2009) 3656.
[50] A. Bodi, J.P. Kercher, C. Bond, P. Meteesatien, B. Sztaray, T. Baer, J. Phys. Chem. A 110 (2006) 13425.
[51] E.A. Fogleman, H. Koizumi, J.P. Kercher, B. Sztaray, T. Baer, J. Phys. Chem. A 108 (2004) 5288.
[52] W.R. Roth, F. Bauer, A. Beitat, T. Ebbrecht, M. Wustefeld, Chem. Ber. 124 (1991) 1453.
[53] D.W. Kohn, H. Clauberg, P. Chen, Rev. Sci. Instrum. 63 (1992) 4003.
[54] A.V. Friderichsen, J.G. Radziszewski, M.R. Nimios, P.R. Winter, D.C. Dayton, D.E. David, G.B. Ellison, J. Am. Chem. Soc. 123 (2001) (1977).
[55] H. Clauberg, D.W. Minsek, P. Chen, J. Am. Chem. Soc. 114 (1992) 99.
[56] M.J. Frisch, G.W. Trucks, H.B. Schlegel, G.E. Scuseria, M.A. Robb, J.R. Cheeseman, J.A. Montgomery, Jr., T. Vreven, K.N. Kudin, J.C. Burant, J.M. Millam, S.S. Iyengar, J. Tomasi, V. Barone, B. Mennucci, M. Cossi, G. Scalmani, N. Rega, G.A. Petersson, H. Nakatsuji, M. Hada, M. Ehara, K. Toyota, R. Fukuda, J Hasegawa, M. Ishida, T. Nakajima, Y. Honda, O. Kitao, H. Nakai, M. Klene, X. Li, J.E. Knox, H.P. Hratchian, J.B. Cross, V. Bakken, C. Adamo, J. Jaramillo, R. Gomperts, R.E. Stratmann, O. Yazyev, A.J. Austin, R.; Cammi, C. Pomelli, J.W. Ochterski, P.Y. Ayala, K. Morokuma, G.A. Voth, P. Salvador, J.J. Dannenberg, V.G. Zakrzewski, S. Dapprich, A.D. Daniels, M.C. Strain, O. Farkas, D.K. Malick, A.D. Rabuck, K. Raghavachari, J.B. Foresman, J.V. Ortiz, Q. Cui, A.G. Baboul, S. Clifford, J. Cioslowski, B.B. Stefanov, G. Liu, A. Liashenko, P. Piskorz, I. Komaromi, R.L. Martin, D.J. Fox, T. Keith, M.A. Al-Laham, C.Y. Peng, A. Nanayakkara, M. Challacombe, P.M.W. Gill, B. Johnson, W. Chen, M.W. Wong, C. Gonzalez, J.A. Pople, J.A. Gaussian 03, Revision C.02, Gaussian, Inc., Wallingford CT, 2004.
[57] A.D. Becke, J. Chem. Phys. 109 (2001) 9287.
[58] T.C. Zhang, L.D. Zhang, J. Wang, T. Yuan, X. Hong, F. Qi, J. Phys. Chem. A 112 (2008) 10495.
[59] J.C. Traeger, T.H. Morton, J. Phys. Chem. A 109 (2005) 10467.
[60] W. Tao, R.B. Klemm, F.L. Nesbitt, J.L. Stief, J. Phys. Chem. 96 (1992) 104.
[61] A. Vasiliou, M.R. Nimlos, J.W. Daily, G.B. Ellison, J. Phys. Chem. A 113 (2009) 8540.
[62] K. Sato, Y. Hidaka, Combust. Flame 122 (2000) 291.
[63] J. Ernst, K. Spindler, H.G. Wagner, Ber. Bunsen-Gesell. 80 (1976) 645–650.
[64] S. Saxena, J.H. Kiefer, S.J. Klippenstein, Proc. Combust. Inst. 32 (2009) 123.
[65] L.B. Harding, S.J. Klippenstein, J. Phys. Chem. Lett. 1 (2010) 3016.